APL Materials

Facile synthesis of MoS_2 and $Mo_xW_{1-x}S_2$ triangular monolayers

Cite as: APL Mater. **2**, 092514 (2014); https://doi.org/10.1063/1.4895469
Submitted: 18 July 2014 • Accepted: 29 August 2014 • Published Online: 11 September 2014

Zhong Lin, Michael T. Thee, Ana Laura Elías, et al.

Facile synthesis of MoS_2 and $Mo_xW_{1-x}S_2$ triangular monolayers

Zhong Lin,[1] Michael T. Thee,[1] Ana Laura Elías,[1] Simin Feng,[1] Chanjing Zhou,[2] Kazunori Fujisawa,[1] Néstor Perea-López,[1] Victor Carozo,[1] Humberto Terrones,[3] and Mauricio Terrones[1,2,4,a]

[1]*Department of Physics and Center for 2Dimensional and Layered Materials, The Pennsylvania State University, University Park, Pennsylvania 16802, USA*
[2]*Department of Materials Science and Engineering, The Pennsylvania State University, University Park, Pennsylvania 16802, USA*
[3]*Department of Physics, Applied Physics and Astronomy, Rensselaer Polytechnic Institute, Troy, New York 122180, USA*
[4]*Department of Chemistry, The Pennsylvania State University, University Park, Pennsylvania 16802, USA*

(Received 18 July 2014; accepted 29 August 2014; published online 11 September 2014)

Single- and few-layered transition metal dichalcogenides, such as MoS_2 and WS_2, are emerging two-dimensional materials exhibiting numerous and unusual physico-chemical properties that could be advantageous in the fabrication of unprecedented optoelectronic devices. Here we report a novel and alternative route to synthesize triangular monocrystals of MoS_2 and $Mo_xW_{1-x}S_2$ by annealing MoS_2 and MoS_2/WO_3 precursors, respectively, in the presence of sulfur vapor. In particular, the $Mo_xW_{1-x}S_2$ triangular monolayers show gradual concentration profiles of W and Mo whereby Mo concentrates in the islands' center and W is more abundant on the outskirts of the triangular monocrystals. These observations were confirmed by atomic force microscopy, and high-resolution transmission electron microscopy, as well as Raman and photoluminescence spectroscopy. The presence of tunable PL signals depending on the $Mo_xW_{1-x}S_2$ stoichiometries in 2D monocrystals opens up a wide range of applications in electronics and optoelectronics. [http://dx.doi.org/10.1063/1.4895469]

Single and few-layer transition metal dichalcogenides (TMDs) in the form MX_2 (M = Mo, W, Nb, Re; X = S, Se, Te), have emerged as exotic two dimensional materials with fascinating properties that complement those of graphene and hexagonal boron nitride (hBN).[1–3] Interestingly, semiconducting TMDs (sTMDs) exhibit layer dependent properties. For example, their electronic structure evolves from indirect bandgap, present in the bulk form, to a direct bandgap material occurring in the monolayer form, thus giving rise to drastic increases in photoluminescence emission.[3–6]Therefore, this finite and direct bandgap in the visible range renders single layered sTMDs suitable materials for optoelectronic applications.[7–10] Another noticeable layer dependent property of TMDs is the symmetry of the crystals.[11] In this context, monolayered TMDs possessing the 2H phase lack of inversion symmetry and, as a result, the Kramers degeneracy is lifted.[11] The broken symmetry enables near-unity valley polarization,[12] and strong second harmonic generation.[13–16] In addition, other rich physical phenomena,[17–19] unique in single and few-layered sTMDs offer versatile chemical properties as well enhanced performance in catalytic reactions, gas sensing, and batteries.[20,21]

The research and application of few layered TMDs greatly depends on the effective methods able to isolate monolayers from bulk crystals and, moreover, on the direct synthesis of flakes or sheets

[a]Author to whom correspondence should be addressed. Electronic mail: mut11@psu.edu

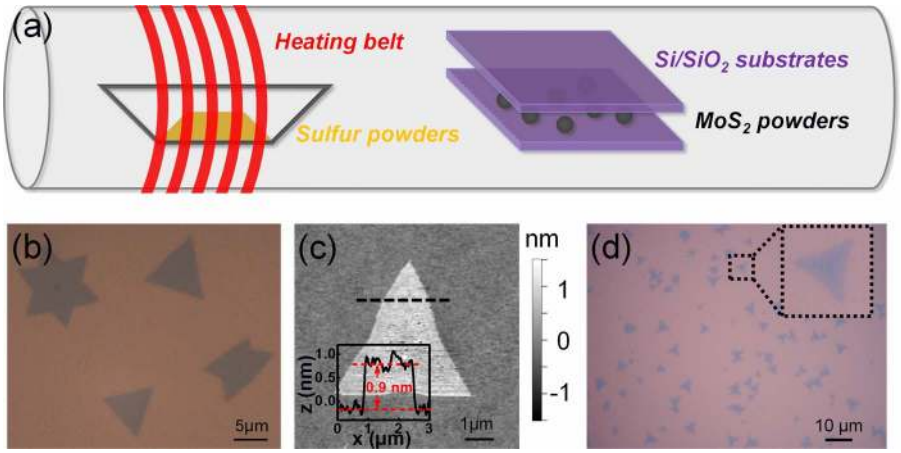

FIG. 1. (a) Schematics showing the synthesis setup for growing MoS_2 and $Mo_xW_{1-x}S_2$ monolayers. MoS_2 or MoS_2/WO_x powders were sandwiched between two SiO_2-Si substrates are loaded into the center of a quartz tube. Sulfur powders were then heated using a heating belt near the inlet of the quartz tube; (b) Optical image of synthesized MoS_2 triangular layers. In addition to triangular islands other morphologies such as David stars and butterflies were observed, and (c) AFM topographic image of a MoS_2 triangular monolayer. The inset shows the height profile measured along the black dashed line; (d) Optical image showing large area synthesis of hybrid $Mo_xW_{1-x}S_2$ monolayers.

with a controlled number of layers. Considerable efforts have been devoted to producing thin layers by either top down or bottom up approaches.[6,20–30] The exfoliation technique, either mechanical- or liquid-based, can be adapted to produce atomically thin sheets from bulk crystals grown by chemical vapor transport.[31,32] Thermolysis, atomic layer deposition (ALD), and chemical vapor deposition (CVD) constitute bottom up approaches that are advantageous for scalability.[6,22–29] In particular, the CVD process is mainly based on the mild sulfurization of transition metal oxides.[6,20,22,23,28,29,33–35] The synthesis of monolayered islands of MoS_2 has also been achieved by thermally treating MoS_2 powders at low pressures at 900 °C.[30] However, in this work we report an alternative approach to synthesize MoS_2 and $Mo_xW_{1-x}S_2$ monolayers at atmospheric pressures by simply annealing MoS_2 or MoS_2/WO_x powders in the presence of S vapor at temperatures as low as 700 °C in an inert Ar atmosphere. Interestingly, the alloyed monolayers exhibited tunable bandgaps across the monocrystal domains, thus offering exciting opportunities for a variety of tunable electronic and optoelectronic applications.

Figure 1(a) depicts a schematic representation of the synthesis of crystalline monolayers of MoS_2 and $Mo_xW_{1-x}S_2$. A few milligrams of MoS_2 or MoS_2/WO_x powders were loaded in the middle of a quartz reaction tube. The sulfide precursor was then annealed at atmospheric pressure in the presence of sulfur vapors in order to avoid oxidation and using Ar as a carrier gas. MoS_2 mono- and few-layers grew on both the supporting and covering substrates, mainly as triangular islands and with typical lateral sizes of ∼tens of micrometers. The growth of the islands was nucleated without the addition of graphene oxide as a seeding element. As the lateral size of the islands increases, these MoS_2 islands can collide and merge (see Fig. 1(b)), thus forming continuous films containing grain boundaries, an observation that is consistent with previous work on MoS_2 thin layers synthesized by sulfurization of metal oxides.[22,23] A large portion (>70%) of as-grown triangles are monolayers, as confirmed by atomic force microscopy (AFM) measurements. MoS_2 monolayer islands were usually found to be *ca.* 0.9 nm thick (see Fig. 1(c)), an observation which is consistent with the presence of monolayered TMDs.[36] The synthesis method for growing single phase MoS_2 monolayers can also be modified to obtain hybrid $Mo_xW_{1-x}S_2$ triangular monocrystals. For example, when MoS_2/WO_3 mixed powders are used as precursors and the synthesis temperature is raised to 800 °C, triangular monolayers of hybrid phases of MoS_2 and WS_2 can be grown. Figure 1(d) depicts a large scale optical image of the hybrid triangular monolayers grown on SiO_2 substrates. The size of hybrid triangles range from hundreds of nanometers to tens of micrometers. As can be seen from the zoom in image, hybrid monolayers appear with slightly nonhomogeneous optical contrast, which is different from

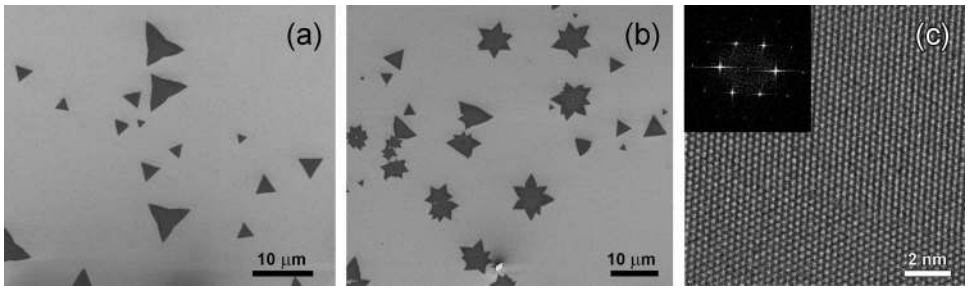

FIG. 2. Electron microscopy images of synthesized MoS_2 monolayered islands. (a) and (b) FESEM micrographs of MoS_2 islands exhibiting different morphologies and sizes. (c) HRTEM image of a triangular island. The inset shows its corresponding FFT pattern.

the case of single phase MoS_2 shown in Fig. 1(b). Few-layered hybrid triangles and continuous films can also by synthesized with prolonged growth time.

Field emission scanning electron microscopy (FESEM) images of the single phase MoS_2 islands are shown in Figs. 2(a) and 2(b). The most common morphology for the monolayers is triangular (3 vertices), but islands with more vertices can also be found among the grown materials. Six pointed stars (David stars) are common, along with five pointed stars and flower-like islands (see Fig. 2(b)). The lateral size of the grown flakes varies from hundreds of nanometers to tens of micrometers. The synthesized MoS_2 monolayers were transferred onto transmission electron microscopy (TEM) grids for further characterization. Figure 2(c) depicts a high-resolution TEM (HRTEM) image of a MoS_2 monolayered island and its corresponding fast Fourier transform (FFT; see inset). A hexagonal pattern can be seen in both the HRTEM and FFT images, indicating the MoS_2 monolayered triangles are highly crystalline and belong to the 2H phase.

Raman spectroscopy has been used as a non-destructive spectroscopy technique to probe sTMDs by studying their vibrational modes. A representative Raman spectrum obtained from monolayered MoS_2 islands synthesized in this work is shown in Fig. 3(a). The recorded Raman spectrum exhibited the characteristic in-plane E′ phonon mode located at 383 cm^{-1} and the out-of-plain A'_1 mode at 404 cm^{-1}. These monolayer modes are analog to the E_{2g} and A_{1g} observed for bulk MoS_2, which exhibits a point group symmetry (D_{6h}) different from that of a monolayer (D_{3h}).[37] It has been demonstrated in exfoliated MoS_2 flakes that the E′ mode is sensitive to local strain.[38] A clear sign of strain has not been found in our pristine MoS_2 monolayer. However, in hybrid $Mo_xW_{1-x}S_2$ monolayers, a significant shift of the E′ mode is noticed and will be discussed later. Besides Raman spectroscopy, PL spectroscopy constitutes another powerful tool to study and identify sTMDs. Figure 3(b) shows a typical PL spectrum of MoS_2 triangles, exhibiting a single sharp peak located at *ca.* 1.81 eV (equivalent to 686 nm), with a full width of the peak at half maximum (FWHM) of 74 meV. Interestingly, the intensity of the PL signal is high when compared to the E′ Raman mode ($I_{PL}/I_{E'} = 56$). This intense PL emission is a result of a direct bandgap present in the monolayer.[5] The B1 excitonic transition, originating from the spin-orbital coupling,[4] is not noticeable in the PL spectrum. A single, sharp, and intense peak in a PL spectrum has been viewed as a sign of high optical quality in mechanically exfoliated and CVD grown sTMD monolayers.[5,6] The monolayers synthesized in this work exhibit comparable quality with exfoliated and CVD monolayers, and could possibly be used in optoelectronic devices.

Figure 3(c) depicts Raman spectra obtained from three different regions of a typical hybrid $Mo_xW_{1-x}S_2$ triangle. The central region and border of this triangle appear with different optical contrasts, implying possible variations in elemental compositions (see Fig. 1(d)). Raman spectra acquired from three spots (center, edge, and border region) clearly indicate changes of phase compositions. In the central region, both MoS_2 and WS_2 phases are present, but the MoS_2 phase dominates (the intensity ratio of A'_1 mode: $I_{WS2}/I_{MoS2} = 0.6$). Near the edge of the monolayered triangle, two phases coexist, while WS_2 becomes the dominating phase (the intensity ratio of A'_1 mode: $I_{WS2}/I_{MoS2} = 7.8$). Within the single domain, the Raman modes could shift by several wavenumbers. For example, from the center to the edge region, the peak position of MoS_2-like E′ mode shifts

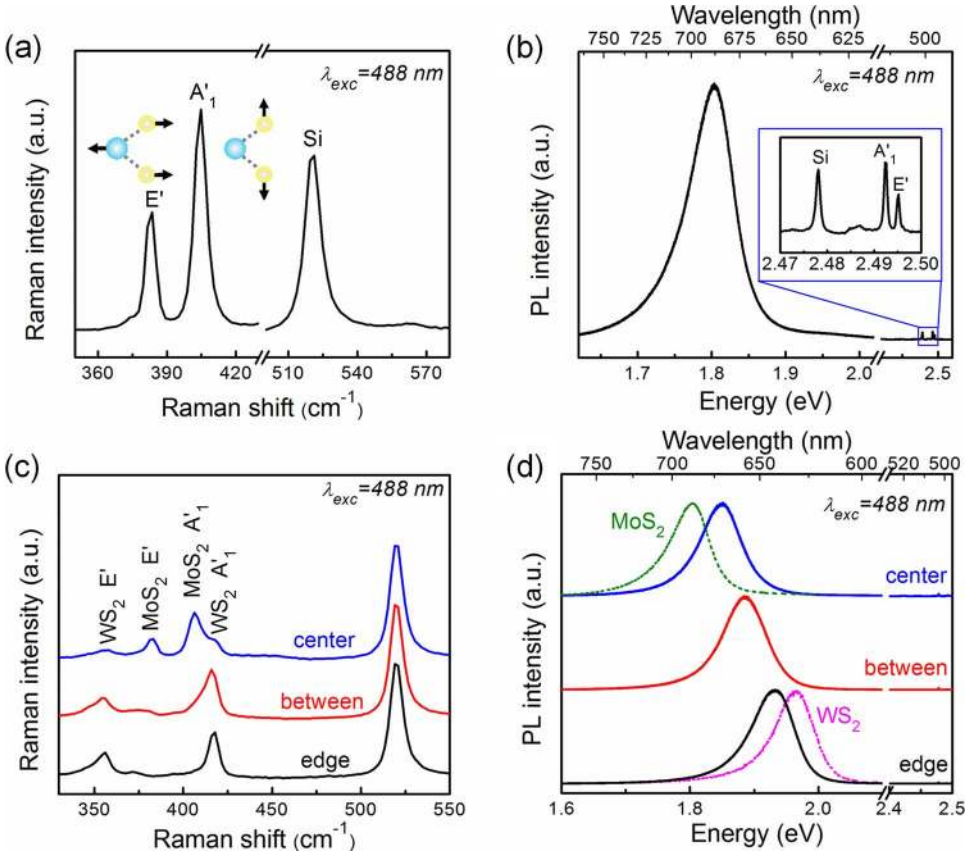

FIG. 3. Comparison of single phase and hybrid monolayers from point spectra. (a) Raman spectrum of triangular MoS_2 monolayers. The inset shows schematics of in-plane and out-of-plane Raman modes; (b) PL spectrum of MoS_2 monolayers. The zoom-in view depicts the Raman peaks; (c) Raman spectra of a hybrid $Mo_xW_{1-x}S_2$ monolayer. Raman spectra are acquired from the center, intermediate region, and edge of a hybird triangle. Raman intensity has been normalized to the Si peak (substrate). (d) Normalized PL spectra acquired from three locations of the same hybrid $Mo_xW_{1-x}S_2$ triangular monolayer. Raman modes are the weak peaks near 2.5 eV. The Raman intensity is much weaker than the PL intensity, indicting the hybrid triangle is monolayer.[5,6] PL spectra of single phase MoS_2 and WS_2 monolayers are also plotted with dashed lines in (d) as references. MoS_2 monolayers are grown with the method proposed in current work. WS_2 monolayers are grown by sulfurizing thermally deposited WO_x films.[6]

from 383 to 373 cm^{-1}, and the separation between MoS_2-like E′ and A'_1 modes changes from 24 to 33 cm^{-1}. These Raman shifts may be associated with local strain induced by mixing two phases with different lattice constants, and the shift trends are similar to those reported in uniform alloys of MoS_2 and WS_2 produced by chemical vapor transport.[39] Regarding the growth of our hybrid monocrystalline islands, a possible formation mechanism is described as follows: A MoS_2 monolayer starts to nucleate on defective regions of the SiOx substrate at temperatures close to 700 ° C,[23] once MoS_2 starts growing outwardly, units of WS_2 liberated at higher temperatures around 800 °C, start to deposit on the growing edges of MoS_2.[6,34] Therefore, MoS_2 nucleates first and facilitates the subsequent lateral growth of WS_2. In agreement with the compositional changes shown by Raman spectroscopy, a gradual change in the bandgap is observed from different PL spectra. From the center to the edge of the hybrid triangle, the PL spectrum is dominated by a single and intense peak with the PL peak energy varies from 1.85 eV to 1.93 eV (see Fig. 3(d)), whereas the FWHM of the peaks remains unchanged (*ca.* 80 meV). The peak energies on the center and the edge neither coincide exactly with the bandgap of pure phase MoS_2 (1.81 eV in current work; see dotted line in Fig. 3(d)) nor with pure WS_2 (1.97 eV; see dotted line in Fig. 3(d)), possibly due to an alloying effect within $Mo_xW_{1-x}S_2$ domains.

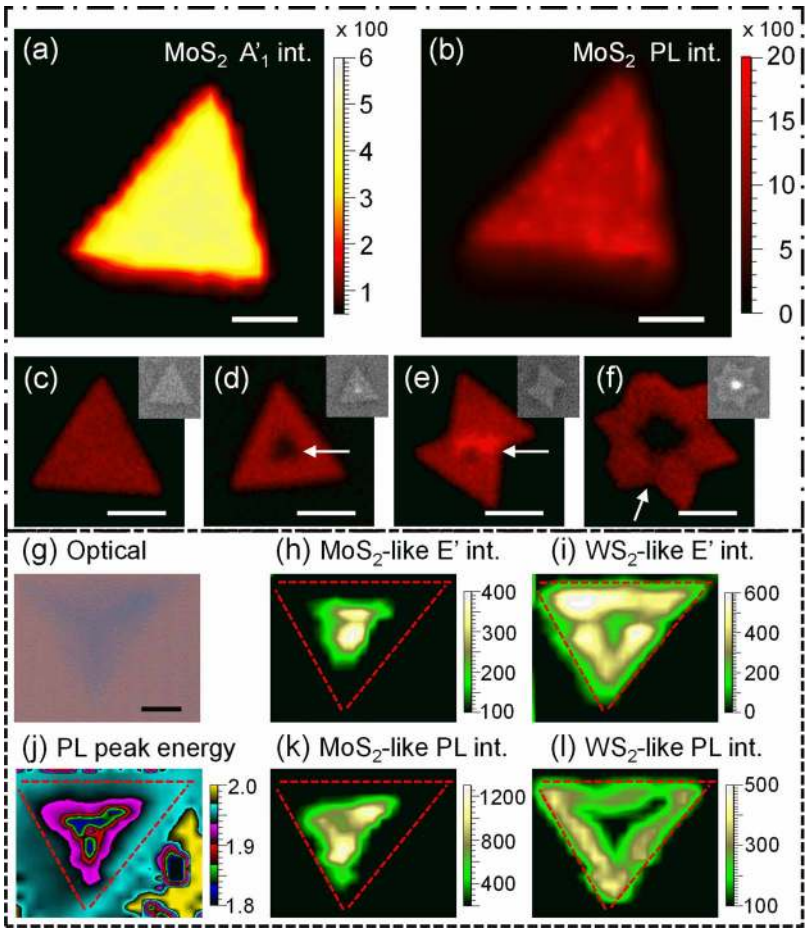

FIG. 4. Comparison of single phase (upper panel) and hybrid (lower panel) monolayers from mappings. (a) Intensity map of the A'_1 Raman mode in single phase MoS_2, and (b) intensity map of the characteristic PL peak centered at *ca.* 1.81 eV in single phase MoS_2. The scale bars are 2 μm in (a) and (b); (c)–(f) are fluorescence images taken from MoS_2 monolayers with various morphologies. The corresponding optical images are shown as insets with defective features indicated by arrows: (c) uniform triangle, (d) triangle with a nucleation center, (e) polycrystalline "butterfly" with a tilt boundary, (f) polycrystalline "David star" with mirror boundaries. The scale bar in (c)–(f) is 5 μm. (c)–(f) are shown on the same color scale. The mappings performed on hybrid triangles are summarized in the lower panel. (g) Optical image of a hybrid $Mo_xW_{1-x}S_2$ monolayer used for mapping. The scale bar is 2 μm; (h) Raman intensity map of the MoS_2-like E′ mode; (i) Raman intensity map of the WS_2-like E′ mode; (j) PL map showing the peak energy in unit of eV; (k) PL intensity map at a fixed energy of 1.81 eV, corresponding to the bandgap of single phase MoS_2 monolayers; (l) PL intensity map at a fixed energy of 1.97 eV, corresponding to the bandgap of single phase WS_2 monolayers. The laser excitation was 488 nm and this was used for Raman and PL measurements.

Besides point spectral acquisitions, Raman and PL mappings were also recorded by scanning the focused laser across the triangular islands. Based on mappings shown in Fig. 4, we compared single phase MoS_2 with hybrid $Mo_xW_{1-x}S_2$ monolayers. As shown in Figs. 4(a) and 4(b), the Raman and PL intensities across a single phase MoS_2 domain are uniform, further demonstrating the high optical quality of MoS_2 monolayers synthesized by the simple annealing of MoS_2 powders. It is important to note that this method does not result in the enhanced edge PL emission and this observation could be due to the different chemical functionalization of metal oxides usually used for edge-enhanced PL TMD synthesis.[6] Fluorescence microscopy was also employed to study the optical properties of MoS_2 monolayer islands grown into various morphologies, such as triangles, butterflies, and David stars (Figs. 4(c)–4(f)). Fluorescence microscopy is faster and even less destructive when compared to PL mapping, and since PL and fluorescence emissions originate from the same optical process, fluorescence microscopy constitutes an alternative optical technique to identify and characterize sTMDs monolayers. Figures 4(c) and 4(d) depict how the number of layers affects fluorescence

intensity. In the nucleation center of the triangle shown in Fig. 4(d), the fluorescence intensity is quenched as a result of the presence of an indirect bandgap in few-layered MoS_2. Figures 4(e) and 4(f) show aggregated MoS_2 triangles with tilt and mirror boundaries, respectively.[23] The fluorescence signal is enhanced near the tilt boundary, while it is slightly reduced near the mirror boundary, an observation that is consistent with previous results recently reported in the literature.[23]

For hybrid triangles containing MoS_2 and WS_2 phases, the in-plane stoichiometric gradient and bandgap can be directly visualized from Raman and PL maps shown in Figs. 4(g)–4(l). For example, it is possible to observe the dominating phase changes gradually from the center to the edge of triangles. When comparing Figs. 4(g), 4(k), and 4(l), it is clear the less transparent region shown in the optical image is rich in MoS_2 phase. The gradual change in bandgap can also be observed from the PL peak energy map (see Fig. 4(j)). It is noteworthy that this work reports the synthesis of a novel two-dimensional material with a continuously tunable direct bandgap within the same monocrystalline domain, which differs from previous reports synthesizing homogeneous alloys of WS_2 and MoS_2. Although ternary 2D uniform alloys were reported, such as $Mo_xW_{1-x}S_2$ alloy grown by chemical vapor transport, and MoS_xSe_{2-x} grown by CVD, the bandgap is unchanged across the domains because Mo/W or S/Se atoms are randomly or homogenously distributed within samples, as confirmed by scanning transmission electron microscopy (STEM).[39–41] However, in the hybrid $Mo_xW_{1-x}S_2$ triangles synthesized in this work, the composition of Mo–W is gradual, thus leading to an in-plane tunable bandgap material. Considering the difference between bandgaps, work functions, and carrier mobilities between MoS_2 and WS_2, the hybrid structure could offer new alternative and attractive materials in electronics and optoelectronics.[42–44]

The experimental details about material syntheses and characterizations are described below. Monolayer islands of MoS_2 and $Mo_xW_{1-x}S_2$ were grown by atmospheric pressure CVD at 700 and 800 °C, respectively. In particular, Si wafers with a 300 nm Si/SiO_2 layer, cleaned with a H_2SO_4/H_2O_2 solution (mixed in 3:1), were used as substrates. An alumina boat containing 300 mg sulfur (Alfa Aesar, 99.5%) was located upstream and was independently heated using a heating tape. In order to grow MoS_2 monolayers, 5 mg of MoS_2 powder (Sigma Aldrich, particle size ~6 μm) was placed directly on a Si/SiO_2 substrate and another wafer was placed directly on top of it with the shiny SiO_2 side facing down. For MoS_2 growth, the furnace was heated up with the following temperature ramp: heated up to 500 °C in 20 min, then heated to 700 °C in the subsequent 20 min with a dwell time of 30 min, and subsequently the system was allowed to cool down to room temperature. For growing $Mo_xW_{1-x}S_2$ hybrid monolayers, 2 mg of WO_3 powder (Alfa Aesar, 99.998%) was covered with 4 mg of MoS_2 powder (Sigma Aldrich, particle size ~6 μm), and placed between the two Si/SiO_2 substrates as explained above. The furnace heating ramp for $Mo_xW_{1-x}S_2$ was controlled as follows: heated to 500 °C in 20 min, then heated to 800 °C in the following 20 min, and the dwell time was set to 30 min. Sulfur powder was heated separately in both syntheses with the following heating ramp: heat up to 70 °C in 10 min with a 30 min dwell time, then the ramp increased the temperature to 250 °C in the subsequent 6 min, and a 20 min dwell time followed by naturally cooling the system down to room temperature. The quartz reaction tube was flushed with 300 sccm high purity Ar for 20 min in order to remove oxygen before the growth process started. A 100 sccm of Ar were used during the synthesis. It should be noted that MoS_2 and $Mo_xW_{1-x}S_2$ monolayer triangles grew on both the bottom and top substrates. After syntheses, residual powders on the substrate were removed ultrasonically in acetone.

The AFM characterization was performed with MFP-3D AFM by Asylum Research with non-contact tapping mode.

As grown MoS_2 islands were imaged using a FEI Nova NanoSEM 630, operated at 5 kV.

The MoS_2 islands grown on substrates were first spin coated with a poly(methyl methacrylate) (PMMA) layer and then immersed into NaOH 1M at 80 °C to lift off the islands. After washing away the NaOH with deionized water, the PMMA-MoS_2 films were then fished onto a quantifoil© Au TEM grid. In order to remove PMMA residues, the grid was cleaned with acetone and then annealed at 350 °C in Ar.

The HRTEM was performed in a JEOL 2010F TEM equipped with a field emission source and an ultrahigh resolution pole piece (Cs = 0.5 nm). An accelerating voltage at 200 kV was used for imaging.

Raman and PL spectra acquisition were carried out using an inVia confocal Renishaw Raman spectrometer. A 100× objective lens and a 488 nm laser wavelength were used to excite the samples. The spectrometer was calibrated with a standard Si sample before the measurements. In order to perform Raman and PL mappings, a focused laser spot was scanned over the sample surfaces with a step size of 0.3 μm.

Fluorescence images were recorded with a Carl Zeiss Axio Imager microscope under a 50× objective. The illumination light was generated from an X-Cite Series 120Q white light source, and was filtered to allow green light to pass. The emitted red fluorescent light was collected using a gray scale CCD. The images were artificially colored in red.

This work was funded by the U.S. Army Research Office under MURI ALNOS project, Contract/Grant No. W911NF-11-1-0362. M.T. acknowledges Penn State Center for Nanoscale Science for the seed grant on 2D Layered Materials (DMR-0820404), and Center for two-Dimensional and Layered Materials at The Pennsylvania State University.

[1] K. Novoselov, D. Jiang, F. Schedin, T. Booth, V. Khotkevich, S. Morozov, and A. Geim, Proc. Natl. Acad. Sci. U.S.A. **102**, 10451 (2005).
[2] S. Z. Butler, S. M. Hollen, L. Cao, Y. Cui, J. A. Gupta, H. R. Gutiérrez, T. F. Heinz, S. S. Hong, J. Huang, A. F. Ismach, E. Johnston-Halperin, M. Kuno, V. V. Plashnitsa, R. D. Robinson, R. S. Ruoff, S. Salahuddin, J. Shan, L. Shi, M. G. Spencer, M. Terrones, W. Windl, and J. E. Goldberger, ACS Nano **7**, 2898 (2013).
[3] M. Xu, T. Liang, M. Shi, and H. Chen, Chem. Rev. **113**, 3766 (2013).
[4] A. Splendiani, L. Sun, Y. Zhang, T. Li, J. Kim, C. Y. Chim, G. Galli, and F. Wang, Nano Lett. **10**, 1271 (2010).
[5] K. F. Mak, C. Lee, J. Hone, J. Shan, and T. F. Heinz, Phys. Rev. Lett. **105**, 136805 (2010).
[6] H. R. Gutiérrez, N. Perea-López, A. L. Elías, A. Berkdemir, B. Wang, R. Lv, F. López-Urías, V. H. Crespi, H. Terrones, and M. Terrones, Nano Lett. **13**, 3447 (2013).
[7] O. Lopez-Sanchez, D. Lembke, M. Kayci, A. Radenovic, and A. Kis, Nat. Nanotechnol. **8**, 497 (2013).
[8] N. Perea-López, Z. Lin, N. R. Pradhan, A. Iñiguez-Rábago, A. L. Elías, A. McCreary, J. Lou, P. M. Ajayan, H. Terrones, L. Balicas, and M. Terrones, 2D Materials **1**, 011004 (2014).
[9] N. Perea-López, A. L. Elías, A. Berkdemir, A. Castro-Beltran, H. R. Gutiérrez, S. Feng, R. Lv, T. Hayashi, F. López-Urías, S. Ghosh, B. Muchharia, S. Talapatra, H. Terrones, and M. Terrones, Adv. Funct. Mater. **23**, 5511 (2013).
[10] L. Britnell, R. Ribeiro, A. Eckmann, R. Jalil, B. Belle, A. Mishchenko, Y. J. Kim, R. Gorbachev, T. Georgiou, S. Morozov, A. N. Grigorenko, A. K. Geim, C. Casiraghi, A. H. Castro Neto, and K. S. Novoselov, Science **340**, 1311 (2013).
[11] Q. H. Wang, K. Kalantar-Zadeh, A. Kis, J. N. Coleman, and M. S. Strano, Nat. Nanotechnol. **7**, 699 (2012).
[12] X. Xu, W. Yao, D. Xiao, and T. F. Heinz, Nat. Phys. **10**, 343 (2014).
[13] C. Janisch, Y. Wang, D. Ma, N. Mehta, A. L. Elías, N. Perea-López, M. Terrones, V. Crespi, and Z. Liu, Sci. Rep. **4**, 5530 (2014).
[14] Y. Li, Y. Rao, K. F. Mak, Y. You, S. Wang, C. R. Dean, and T. F. Heinz, Nano Lett. **13**, 3329 (2013).
[15] C. Janisch, N. Mehta, D. Ma, A. L. Elías, N. Perea-López, M. Terrones, and Z. Liu, Opt. Lett. **39**, 383 (2014).
[16] N. Kumar, S. Najmaei, Q. N. Cui, F. Ceballos, P. M. Ajayan, J. Lou, and H. Zhao, Phys. Rev. B **87**, 161403(R) (2013).
[17] A. Geim and I. Grigorieva, Nature (London) **499**, 419 (2013).
[18] H. Terrones, F. López-Urías, and M. Terrones, Sci. Rep. **3**, 1549 (2013).
[19] H. Terrones and M. Terrones, 2D Materials **1**, 011003 (2014).
[20] X. Huang, Z. Zeng, and H. Zhang, Chem. Soc. Rev. **42**, 1934 (2013).
[21] M. Chhowalla, H. S. Shin, G. Eda, L. J. Li, K. P. Loh, and H. Zhang, Nat. Chem. **5**, 263 (2013).
[22] S. Najmaei, Z. Liu, W. Zhou, X. Zou, G. Shi, S. Lei, B. I. Yakobson, J.-C. Idrobo, P. M. Ajayan, and J. Lou, Nat. Mater. **12**, 754 (2013).
[23] A. M. van der Zande, P. Y. Huang, D. A. Chenet, T. C. Berkelbach, Y. M. You, G. H. Lee, T. F. Heinz, D. R. Reichman, D. A. Muller, and J. C. Hone, Nat. Mater. **12**, 554 (2013).
[24] Y. Shi, W. Zhou, A.-Y. Lu, W. Fang, Y. H. Lee, A. L. Hsu, S. M. Kim, K. K. Kim, H. Y. Yang, and L. J. Li, Nano Lett. **12**, 2784 (2012).
[25] J. G. Song, J. Park, W. Lee, T. Choi, H. Jung, C. W. Lee, S. H. Hwang, J. M. Myoung, J. H. Jung, S. H. Kim, C. Lansalot-Matras, and H. Kim, ACS Nano **7**, 11333 (2013).
[26] J. K. Huang, J. Pu, C. L. Hsu, M. H. Chiu, Z. Y. Juang, Y. H. Chang, W. H. Chang, Y. Iwasa, T. Takenobu, and L. J. Li, ACS Nano **8**, 923 (2014).
[27] Y. Zhan, Z. Liu, S. Najmaei, P. M. Ajayan, and J. Lou, Small **8**, 966 (2012).
[28] Y. H. Lee, X. Q. Zhang, W. Zhang, M. T. Chang, C. T. Lin, K. D. Chang, Y. C. Yu, J. T. W. Wang, C. S. Chang, and L. J. Li, Adv. Mater. **24**, 2320 (2012).
[29] Y. Yu, C. Li, Y. Liu, L. Su, Y. Zhang, and L. Cao, Sci. Rep. **3**, 1866 (2013).
[30] S. Wu, C. Huang, G. Aivazian, J. S. Ross, D. H. Cobden, and X. Xu, Acs Nano **7**, 2768 (2013).
[31] D.-M. Tang, D. G. Kvashnin, S. Najmaei, Y. Bando, K. Kimoto, P. Koskinen, P. M. Ajayan, B. I. Yakobson, P. B. Sorokin, J. Lou, and D. Golberg, Nat. Commun. **5**, 3631 (2014).
[32] J. N. Coleman, M. Lotya, A. O'Neill, S. D. Bergin, P. J. King, U. Khan, K. Young, A. Gaucher, S. De, and R. J. Smith, Science **331**, 568 (2011).

[33] Y. Feldman, E. Wasserman, D. Srolovitz, and R. Tenne, Science **267**, 222 (1995).
[34] A. L. Elías, N. Perea-López, A. Castro-Beltrán, A. Berkdemir, R. Lv, S. Feng, A. D. Long, T. Hayashi, Y. A. Kim, M. Endo, H. R. Gutierrez, N. R. Pradhan, L. Balicas, T. E. Mallouk, F. Lopez-Urias, H. Terrones, and M. Terrones, ACS Nano **7**, 5235 (2013).
[35] X. Wang, H. Feng, Y. Wu, and L. Jiao, J. Am. Chem. Soc. **135**, 5304 (2013).
[36] T. Wieting and J. Verble, Phys. Rev. B **3**, 4286 (1971).
[37] H. Terrones, E. Del Corro, S. Feng, J. Poumirol, D. Rhodes, D. Smirnov, N. Pradhan, Z. Lin, M. Nguyen, A. Elías, T. E. Mallouk, L. Balicas, M. A. Pimenta, and M. Terrones, Sci. Rep. **4**, 4215 (2014).
[38] C. Rice, R. J. Young, R. Zan, U. Bangert, D. Wolverson, T. Georgiou, R. Jalil, and K. S. Novoselov, Phys. Rev. B **87**, 081307(R) (2013).
[39] Y. Chen, J. Xi, D. O. Dumcenco, Z. Liu, K. Suenaga, D. Wang, Z. Shuai, Y. Huang, and L. Xie, Acs Nano **7**, 4610 (2013).
[40] Y. Gong, Z. Liu, A. Lupini, G. Shi, J. Lin, S. Najmaei, Z. Lin, A. L. Elías, A. Berkdemir, G. You, H. Terrones, M. Terrones, R. Vajtai, S. T. Pantelides, S. J. Pennycook, J. Lou, W. Zhou, and P. M. Ajayan, Nano Lett. **14**, 442 (2014).
[41] Q. Feng, Y. Zhu, J. Hong, M. Zhang, W. Duan, N. Mao, J. Wu, H. Xu, F. Dong, F. Lin, C. Jin, C. Wang, J. Zhang, and L. Xie, Adv. Mater. **26**, 2648 (2014).
[42] B. Radisavljevic, A. Radenovic, J. Brivio, V. Giacometti, and A. Kis, Nat. Nanotechnol. **6**, 147 (2011).
[43] W. Zhu, T. Low, Y. H. Lee, H. Wang, D. B. Farmer, J. Kong, F. Xia, and P. Avouris, Nat. Commun. **5**, 3087 (2014).
[44] H. Schmidt, S. Wang, L. Chu, M. Toh, R. Kumar, W. Zhao, A. H. Castro Neto, J. Martin, S. Adam, B. özyilmaz, and G. Eda, Nano Lett. **14**, 1909 (2014).